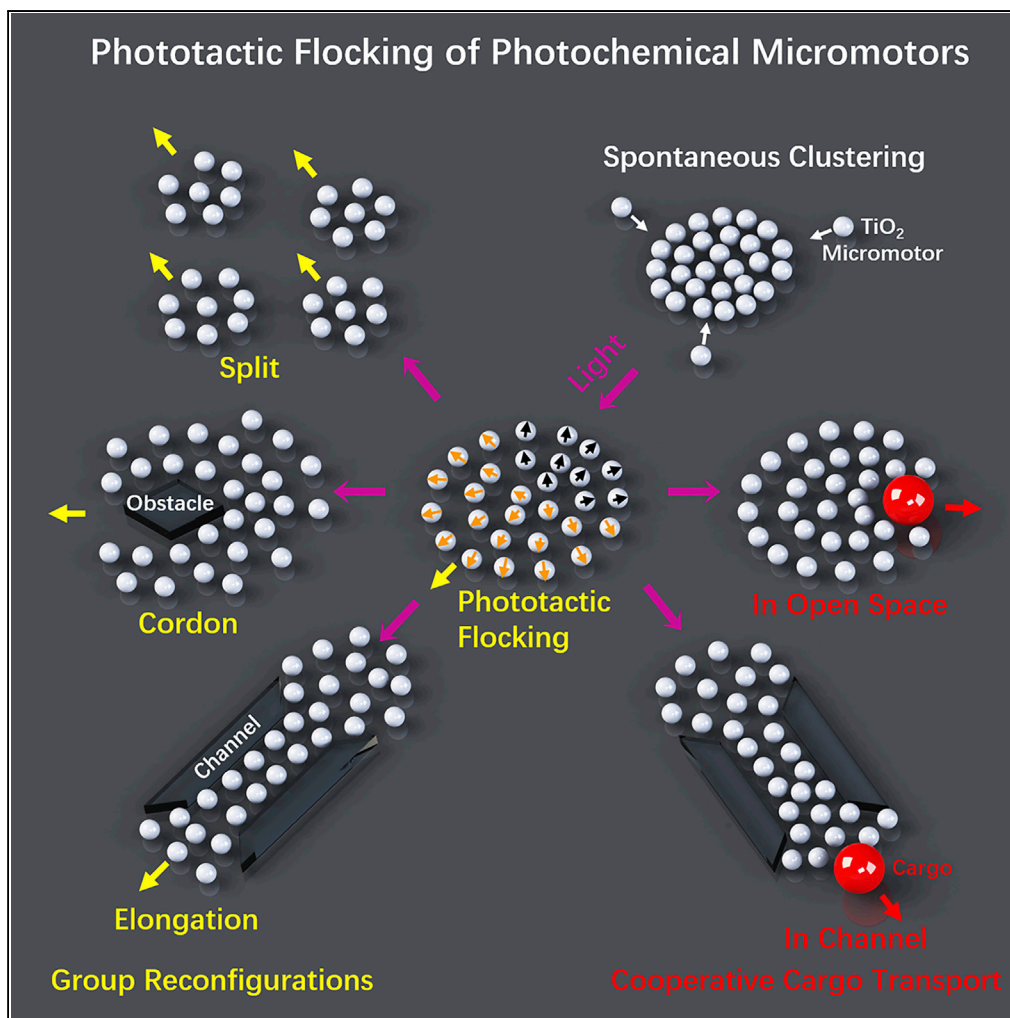


Article

Phototactic Flocking of Photochemical Micromotors



Fangzhi Mou,
Jianhua Zhang,
Zhen Wu, Sinan
Du, Zexin Zhang,
Leilei Xu, Jianguo
Guan

zhangzx@suda.edu.cn (Z.Z.)
guanji@whut.edu.cn (J.G.)

HIGHLIGHTS

TiO₂ micromotors with rich hydroxyl groups can spontaneously gather into flocks

The flocks exhibit dilatational negative phototaxis and adaptive reconfigurations

The flocks can migrate along pre-designed paths and actively bypass obstacles

The flocks can execute cooperative cargo transport and collective mapping

Mou et al., iScience 19, 415–424
September 27, 2019 © 2019
The Author(s).
<https://doi.org/10.1016/j.isci.2019.07.050>

Article

Phototactic Flocking of Photochemical Micromotors

Fangzhi Mou,^{1,3} Jianhua Zhang,^{1,3} Zhen Wu,¹ Sinan Du,² Zexin Zhang,^{2,*} Leilei Xu,¹ and Jianguo Guan^{1,4,*}

SUMMARY

Inspired by astonishing collective motions and tactic behaviors in nature, here we show phototactic flocking of synthetic photochemical micromotors. When enriched with hydroxyl groups, TiO₂ micromotors can spontaneously gather into flocks in aqueous media through electrolyte diffusiophoresis. Under light irradiation, due to the dominant nonelectrolyte diffusiophoretic interaction resulting from the overlap of asymmetric nonelectrolyte clouds around adjacent individuals, these flocks exhibit intriguing collective behaviors, such as dilatational negative phototaxis, high collective velocity, and adaptive group reconfiguration. Consequently, the micromotor flocks can migrate along pre-designed paths and actively bypass obstacles with reversible dilatation (expansion/contraction) under pulsed light navigation. Furthermore, owing to the enhanced driving force and rapid dilatational area covering, they are able to execute cooperative tasks that single micromotors cannot achieve, such as cooperative large-cargo transport and collective microenvironment mapping. Our discovery would promote the creation of reconfigurable microrobots, active materials, and intelligent synthetic systems.

INTRODUCTION

In nature, a variety of living organisms, including bacteria, fish, birds, and mammals, can self-organize into large groups through local communications, despite the large differences in size scale and cognition capability (Parrish and Edelstein-Keshet, 1999; Reynolds, 1987; Vicsek and Zafeiris, 2012). Furthermore, the grouping animals may readily undergo adaptive group reconfigurations (such as expansion/contraction, split/fusion, and bend/elongation) in response to environmental cues like predators, foods, and obstacles (Chen et al., 2017a; Schaerf et al., 2017). As a result, they exhibit rich types of emergent phenomena and cooperative functions that individuals do not possess, thus greatly improving the possibility to survive and prosper (Feinerman et al., 2018; Ioannou et al., 2012).

Inspired by such astonishing collective behaviors in nature and motivated by great visions of creating groups of micro/nanorobots to execute complex tasks that individuals cannot achieve, researchers have recently been dedicated to collective behaviors of synthetic micro/nanomotors (Singh et al., 2017; Wang et al., 2015; Wu et al., 2018; Xie et al., 2019; Xu et al., 2015; Yan et al., 2016; Yu et al., 2018) after an in-depth understanding of the propulsion and design of single counterparts (Guix et al., 2014; Li et al., 2016; Moran and Posner, 2017; Sánchez et al., 2015; Wang and Pumera, 2015; Xu et al., 2017). For example, with the introduction of local physical interactions to neighboring individuals under external AC electric, light, acoustic, and oscillating magnetic fields, Janus spheres, bimetallic nanomotors, conductive particles, and magnetic particles have been demonstrated to be aggregated into active chains, clusters, and swarms usually in a passive manner (Aranson and Sapozhnikov, 2004; Deng et al., 2018; Sapozhnikov et al., 2003; Xu et al., 2014; Yan et al., 2016; Yu et al., 2018). In contrast, some chemically powered micromotors, such as SiO₂/TiO₂, AgCl, Ag₃PO₄, and Fe₂O₃/polymer micromotors can sense and respond to signaling chemicals released from their neighboring conspecifics and thus spontaneously gather into clusters or assemblies (Duan et al., 2013; Hong et al., 2010; Ibele et al., 2009; Palacci et al., 2013). However, these chemically powered micromotors without external guidance only show collective positional order through clustering and manifest no significant orientational order in the swimming direction (Zottl and Stark, 2016), making them unable to actively find targets or working sites for fulfilling cooperative tasks as a group.

In analogy to the tactic behavior of living organisms in nature that enables them to move toward or away from the stimulus to find nutrients or escape threats, single tactic micro/nanomotors have been reported to independently achieve self-navigation or self-targeting in unknown or dynamically changing environments for fulfilling tasks (You et al., 2018). Herein, we demonstrate tactic behaviors of grouping micromotors. TiO₂

¹State Key Laboratory of Advanced Technology for Materials Synthesis and Processing, International School of Materials Science and Engineering, Wuhan University of Technology, 122 Luoshi Road, Wuhan 430070, China

²State and Local Joint Engineering Laboratory for Novel Functional Polymeric Materials, College of Chemistry, Chemical Engineering and Materials Science, Soochow University, Suzhou 215123, China

³These authors contributed equally

⁴Lead Contact

*Correspondence: zhangzx@suda.edu.cn (Z.Z.), guanjq@whut.edu.cn (J.G.)
<https://doi.org/10.1016/j.isci.2019.07.050>

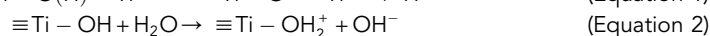


micromotors with rich hydroxyl groups can spontaneously gather into flocks due to the electrolyte diffusio-phoretic attractions resulting from the different diffusivities of the self-secreted electrolyte signals (H^+ and OH^-). The gathered micromotors under light irradiation exhibit intriguing collective behaviors because of the dominant nonelectrolyte diffusio-phoretic interactions. For instance, compared with single micromotors, the flocking micromotors show dilatational negative phototaxis with greatly enhanced collective velocity due to the interparticle accumulation of nonelectrolyte products (i.e., O_2 molecules) and the enhanced concentration gradient across the flock. Furthermore, the micromotor flock can split into multiple subflocks by regrouping the scattered individuals after continuous light irradiation and also reconfigure adaptively in response to local landscapes because of the different individual behaviors near landscape boundaries, including different motion directions and diffusio-phoretic repulsions to near neighbors. Thus, under pulsed UV light navigation, the as-developed flocks can not only collectively migrate along pre-designed paths and actively bypass obstacles but also execute cooperative tasks because of the strong driving force and rapid dilatational area covering, such as cooperatively transporting large cargoes and collectively mapping local microenvironments.

RESULTS

To demonstrate phototactic flocking of synthetic micromotors, we first synthesized spherical anatase TiO_2 microparticles with a diameter of $1.2 \mu m$ as individual micromotors (Figure 1A). The Thermogravimetric-differential scanning calorimeter (TG-DSC) analysis (the right panel in Figure 1A) and quantitative elementary analysis of hydrogen confirm that the TiO_2 micromotors have hydroxyl group content (C_{OH}) as high as 0.94 mmol g^{-1} . The Zeta potential (ζ) of the micromotors is measured to be -17 mV . The TiO_2 micromotors in aqueous media with a concentration (C_p) of 0.35 mg mL^{-1} spontaneously attract near neighbors near a glass substrate and gradually gather into small flocks (see Figure S1A and Video S1) and eventually grow into large flocks with an average diameter of $50 \mu m$ within 2 min (Figure 1B). The diameter of the flocks increases with C_p , and no flocks can be formed if C_p decreases to 0.15 mg mL^{-1} (see Figure S1B).

The spontaneous clustering of the TiO_2 micromotors is closely associated with C_{OH} . TiO_2 micromotors with high C_{OH} dispersed in water simultaneously secrete H^+ ions from surface acidic bridging hydroxyls ($pK_a = 2.9$) and OH^- ions from basic terminal hydroxyls ($pK_a = 12.7$) by dissociating water, respectively, as shown in Equations 1 and 2 (Boehm, 1971; Gun'ko et al., 2001; Sugimoto and Zhou, 2002).



Because of the different diffusivities of H^+ ($9.97 \times 10^{-9} \text{ m}^2 \text{ s}^{-1}$) and OH^- ($5.27 \times 10^{-9} \text{ m}^2 \text{ s}^{-1}$), H^+ would diffuse away from the surface of the TiO_2 micromotors much faster than OH^- . Consequently, H^+ and OH^- are unevenly distributed in the local area around the micromotors, and a local electric field (E) is established with a direction pointing to the interspace of neighboring TiO_2 micromotors (black triangles in Figure 1C). This local E then produces a converging electroosmotic flow (Figure 1D) due to the migration of cations in the electrical double layer of TiO_2 micromotors and glass substrate. Along the converging electroosmotic flow (black curves with arrows in Figure 1D), the dispersed TiO_2 micromotors move toward each other to form a small flock, which then attract other adjacent TiO_2 micromotors and grow into a large flock. Thus, the spontaneous clustering of TiO_2 micromotors follows the long-range electrolyte diffusio-phoresis (Hong et al., 2010), in which the electroosmosis dominates the clustering process as the absolute value of ζ of the glass substrate ($\zeta = -85 \text{ mV}$) (Duan et al., 2013) is larger than that of the micromotors ($\zeta = -17 \text{ mV}$), as depicted in Figure S2. On the other hand, the short-range electrostatic repulsions between negatively charged TiO_2 micromotors prevent them from physical contacts and clumping after clustering.

Similar clustering behaviors of the TiO_2 micromotors are observed in the medium without H_2O_2 and in dark, suggesting the negligible effect of H_2O_2 and visible light from the microscope on their clustering, as verified in Figure S3. To further investigate the influence of C_{OH} on the spontaneous clustering of TiO_2 micromotors, TiO_2 micromotors with different C_{OH} are fabricated at different calcination temperatures (T), as shown in Figure S4. The TiO_2 micromotors with C_{OH} of 9.6 and 4.4 mmol g^{-1} , which are obtained at room temperature (RT) and T of 200°C , exhibit an obvious clustering behavior in water. In contrast, the micromotors calcined at T of 650°C ($C_{OH} = 0.036 \text{ mmol g}^{-1}$) manifest no clustering behavior. However, if they are treated with alkaline hydrogen peroxide solution (Wu et al., 2016) to render them with rich hydroxyl groups ($C_{OH} = 0.18 \text{ mmol g}^{-1}$), they could form into flocks again. This result further verifies that the clustering behavior stems from the electrolyte diffusio-phoresis of the hydroxyl-rich TiO_2 micromotors. In

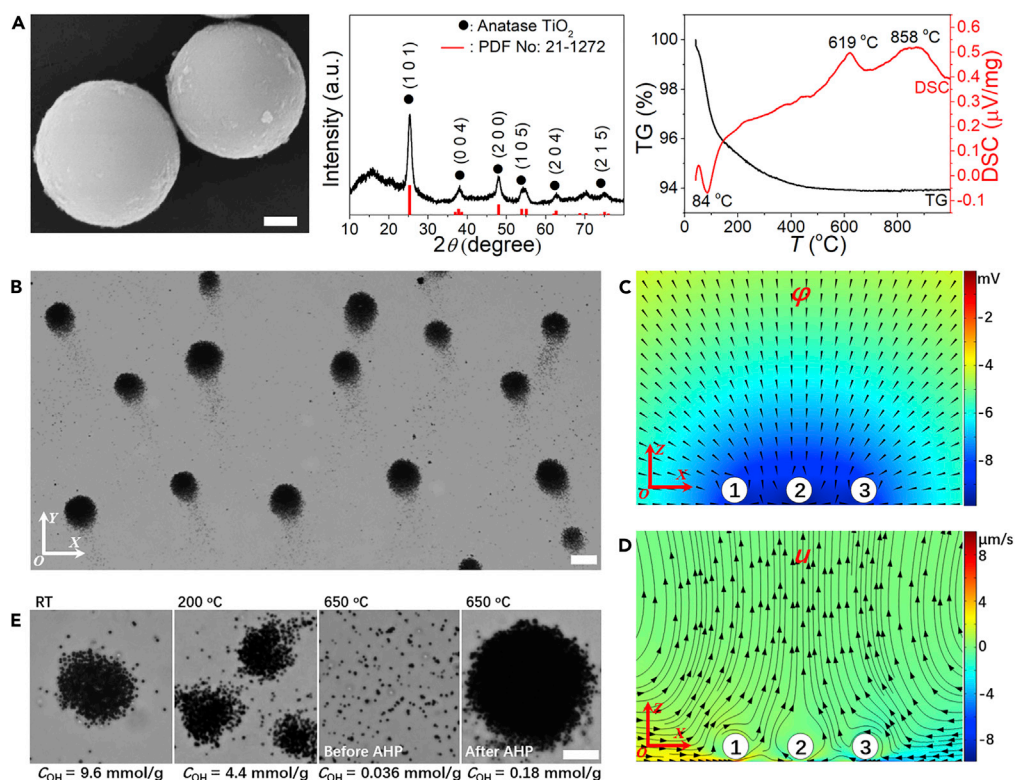


Figure 1. Characterization and Spontaneous Clustering Behaviors of the Micromotors

(A) Scanning electron microscopy (SEM) image, X-ray diffraction (XRD) pattern, and TG-DSC analysis of the TiO₂ micromotors. Scale bar: 200 nm.

(B) TiO₂ micromotor flocks in the aqueous medium with 0.25 wt.% H₂O₂. Scale bar: 20 μm.

(C) Numerical simulation of electric potential (ϕ) resulting from the different diffusivities of the secreted H⁺ and OH⁻ around three TiO₂ micromotors with an interparticle distance of 3 μm. Black triangles indicate the direction of E .

(D) The simulated velocity in the X direction (u) and streamlines (black curves) of the converging hydrodynamic flow induced by the electroosmotic slip of electron double layer of the glass substrate and TiO₂ micromotors under the local E , indicating that TiO₂ micromotor 1 and 3 would move toward 2 along the converging electroosmotic fluid flow.

(E) Clustering behaviors of the micromotors with different C_{OH} obtained at different temperatures, and those obtained at 650 °C after alkaline hydrogen peroxide (AHP) treatment, respectively.

Scale bar: 20 μm.

addition, if the negatively charged glass substrate is replaced by a positively charged glass slide with other conditions unchanged, no clustering behavior is observed for the TiO₂ micromotors, as the electroosmosis, in this condition, tends to drive them to move away from each other (see Figure S5).

After clustering, TiO₂ micromotors show intriguing collective motion behaviors, which are significantly different from the behaviors of the ungrouping (single) ones. When UV is applied sidewise in the Y direction (UV_Y), dispersed single TiO₂ micromotors are activated and moved phototactically as independent micromotors in the same direction (Y axis direction) (Chen et al., 2017b) due to the negligible interaction among them (the left panel in Figure 2A). They stopped immediately and only showed random Brownian motions (the right panel in Figure 2A) when UV was off (see Video S2). In sharp contrast, the TiO₂ micromotors after clustering showed a collective dilatational phototaxis when UV was on. They scattered in all directions and moved away from the light source as a group (see Video S3), in analogy to the asymmetric flash expansion of shoaling fish under an overhead threat (Litvak, 1993). Then, the scattered micromotors aggregate into cohesive flocks again at a new central point after UV is off (see Video S3). Figure 2B shows the time-lapse microscopic images of a typical micromotor flock (top panels) and the corresponding trajectories of individual micromotors (bottom panels), reflecting the dilatational collective order of the flock (Attanasi et al., 2014). It also shows that the flock expands at a normalized rate (r) of 1.2 s⁻¹ under UV_Y irradiation (see Figure S6) and contracts at r of -0.08 s⁻¹ after the UV irradiation stops (Figure 2C). Here the normalized

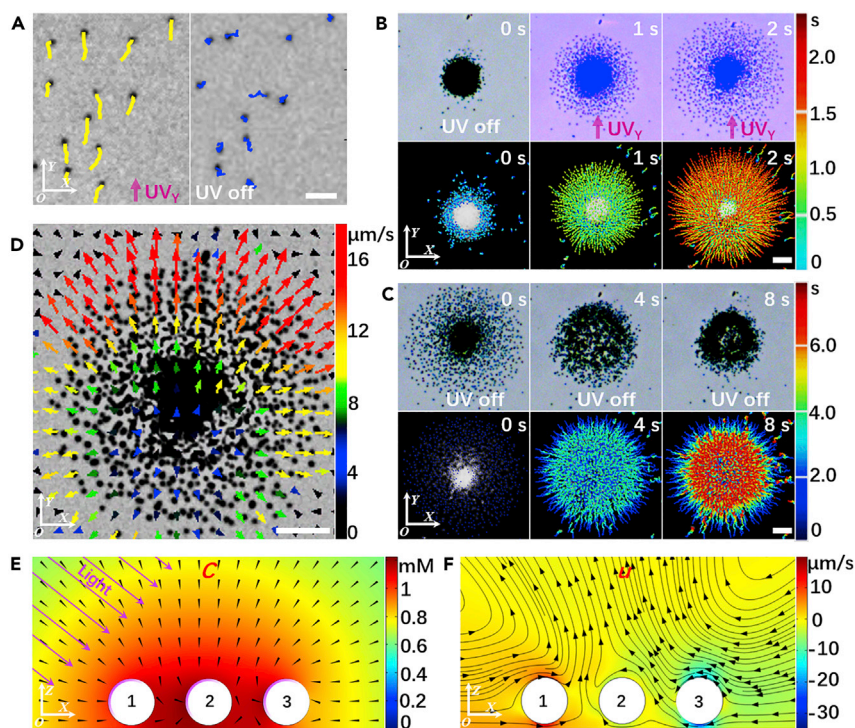


Figure 2. Phototactic Flocking of the Micromotors

(A) Phototactic and Brownian motions of single TiO₂ micromotors when UV_y is on and off, respectively. Images are taken from [Video S2](#). Scale bar: 10 μm.

(B) Optical microscopic images (Top panels) and trajectories (Bottom panels) of the TiO₂ micromotors in a flock under UV_y irradiation. Scale bar: 20 μm.

(C) Optical microscopic images (Top panels) and trajectories (Bottom panels) of the TiO₂ micromotors in a flock when UV_y is turned off. Images in B and C are taken from [Video S3](#). Scale bar: 20 μm.

(D) Instantaneous velocity vectors of the TiO₂ micromotors in a flock when UV_y is on. The length and the color of the arrows denote the magnitude of the velocity, with red and long arrows being the fastest, and dark and short arrows being the slowest. Scale bar: 20 μm.

(E) Steady-state distribution of O₂ concentration (C) around three TiO₂ micromotors with an interparticle distance of 2 μm. Black triangles represent the gradient (∇C) of O₂ concentration. Purple arrows and curves represent the direction of incident UV light and the illuminated surfaces of the micromotors, respectively.

(F) Simulated velocity in the X direction (*u*) and streamlines (black curves) of the hydrodynamic flow induced by ∇C along the surface of the micromotors.

rate $r = (D_t - D_0)/D_0 t$, in which D_0 and D_t are the flock size at a time of 0 s and t , respectively. Instantaneous velocity vectors of individual micromotors in the flock suggest that the micromotors at the forefront of the flock move much faster in the +Y direction than those at the rear end in the -Y direction under UV_y irradiation ([Figure 2D](#)). This implies that the flock moves away from the UV_y stimulus, showing an overall negative phototaxis with a net group velocity (U) of $8.3 \mu\text{m s}^{-1}$. In stark contrast, when the light is applied vertically in z axis direction (UV_z), the flock shows only a size expansion and no population-level motion can be observed (see [Figure S7](#) and [Video S4](#)). It is worth noting that both peripheral individuals ($14 \mu\text{m s}^{-1}$) and the whole flock ($8.3 \mu\text{m s}^{-1}$) show a much higher velocity than the single micromotors ($4.6 \mu\text{m s}^{-1}$, [Figure 2A](#)). These results reveal that, after TiO₂ micromotors gather into groups, intriguing collective behaviors have emerged, involving dilatational negative phototaxis and much-increased velocity of the individuals and the whole group.

To decipher the collective behaviors of the TiO₂ micromotors under UV irradiation, we have constructed a simple numerical model consisting of three TiO₂ micromotors. Under the UV irradiation (purple arrows in [Figure 2E](#)), the photocatalytic decomposition of H₂O₂ occurs asymmetrically on the illuminated and shadowed surfaces of the TiO₂ micromotors (see [Figure S8](#)). Thus, an asymmetric cloud of O₂ molecules is

generated around each TiO₂ micromotor (micromotor 1, 2, and 3 in Figure 2E) (Chen et al., 2017b). With the asymmetric photocatalytic reactions proceeding, asymmetric O₂ clouds overlap and still distribute asymmetrically around the micromotors, as shown in the O₂ concentration (C) field in Figure 2E. The generated O₂ molecules have a lower C at the illuminated side of micromotor 1 but a higher C there for micromotor 2 and 3 compared with the shadowed side. Thus, a gradient field of the generated O₂ concentration (∇C) is formed (black triangles in Figure 2E). The ∇C along the micromotor surface induces a chemiosmotic slip toward the region with high O₂ density and thus propels the micromotor to move toward the opposite direction according to the non-electrolyte diffusiophoresis (Anderson, 1989). The hydrodynamic flow (streamlines, black color) generated by the surface chemiosmotic slip suggests that micromotor 1 moves in the -X direction with v_1 , and micromotor 2 and 3 in the +X direction with v_2 and v_3 (Figure 2F). Their velocity further follows a relationship of $|v_3| > |v_1| > |v_2|$, as verified by the velocity (u) of the chemiosmotic slip in the X direction (Figure 2F). Thus, these micromotors move away from one another, suggesting the obvious repulsive interaction between them based on the non-electrolyte diffusiophoresis. On the other hand, if considering these three micromotors as a whole, in addition to the expansion of the group resulted from the repulsions between individuals, the micromotor group would also show a collective phototaxis because of the polarity in the group velocity ($v_1 + v_2 + v_3 > 0$) in the direction of light irradiation (+X direction). As a result, the expansion and the overall phototaxis of the micromotor flock can be attributed to the dominant effect of nonelectrolyte diffusiophoretic interactions between individual micromotors. The greatly enhanced speed of the peripheral individuals and the whole flock compared with single micromotors can be rationalized by their enhanced nonelectrolyte diffusiophoresis, which stems from the enhanced ∇C across the peripheral individuals and the flock, as confirmed by comparing Figures 2E and 2F with S9A and S9B. At the same light condition as that in Figure 2, passive SiO₂ and polystyrene particles (2 μm in size) only show random Brownian motions (Figure S10 and Video S5) in the aqueous medium with 0.25 wt.% H₂O₂, suggesting that the contribution of light-induced flows is negligible to the flocking of micromotors. When the light is turned off, the production of O₂ molecules stops, and the nonelectrolyte diffusiophoretic interactions between the micromotors diminish and finally vanish. In this condition, the electrolyte diffusiophoretic interactions (see Figure S3) dominate again, and the scattered TiO₂ micromotors would gather into cohesive flocks again.

Because of the alternative dominance of non-electrolyte and electrolyte diffusiophoretic interactions between individuals when light is on and off, respectively, the micromotor flocks are expected to be operated by a pulsed light with a proper duty cycle. When the pulse (light-on time) is less than 10 s, the scattered individuals are clustering toward a single central point over time after UV is off, while they aggregate at multiple central points to form multiple small subflocks before merging into one due to the overexpansion ($D_t/D_0 \geq 500\%$). As expected, the micromotor flock experiences reversible dilatations (expansion/contraction) when it moves phototactically under the pulsed light irradiation with a pulse of 2.5 s and a duty cycle of 16.7% (Figure 3A and see also Video S6). Furthermore, increasing the UV intensity (I) and fuel concentration (C_f) enhances the expansion and phototactic velocity (U) of the flock (Figure 3B and see also Figure S11) because of the improved generation rate of O₂ molecules from the photocatalytic reaction (Mou et al., 2015). The dependence of U on I and C_f follows the Michaelis-Menten law (red curves in Figure 3B), implying that the phototactic flocking is powered by the photocatalytic reaction and the U is controlled by the reaction rate. The plateaus of U suggests that the maximum U of the flock is limited by the maximum rate of the photocatalytic H₂O₂ decomposition determined by total active sites of the flocking TiO₂ micromotors (Solovev et al., 2010). Owing to the unique phototactic motion and reversible dilatations, the TiO₂ micromotor flocks can move along a pre-designed path under pulsed light navigation. The dashed line in the left panel of Figure 3C shows a pre-designed path for a flock. Irradiated by the pulsed UV light with on-off repeating cycles depicted in Figure S12, the flock moves phototactically with reversible dilatations, departs from point 1, then passes way stations 2 and 3, and finally reaches the destination 4 (Figure 3C and see also Video S6). This controlled motion behavior suggests that TiO₂ micromotor flocks could move along a pre-designed path by programming light irradiation.

Besides the phototactic flocking with controlled directions and paths, the TiO₂ micromotors could further reconfigure in response to external stimuli or local landscapes. For instance, under continuous irradiation of UV light for more than 40 s, a micromotor flock (the left panel of Figure 4A) would overexpand up to $D_t/D_0 = 1,500\%$ due to the diffusiophoretic repulsion between individuals. For such an overexpanded flock, the scattered individuals will regroup by preferably attracting their nearest neighbors to form dispersed metastable small subflocks under the diffusiophoretic attraction when UV is turned off. Over 1,100

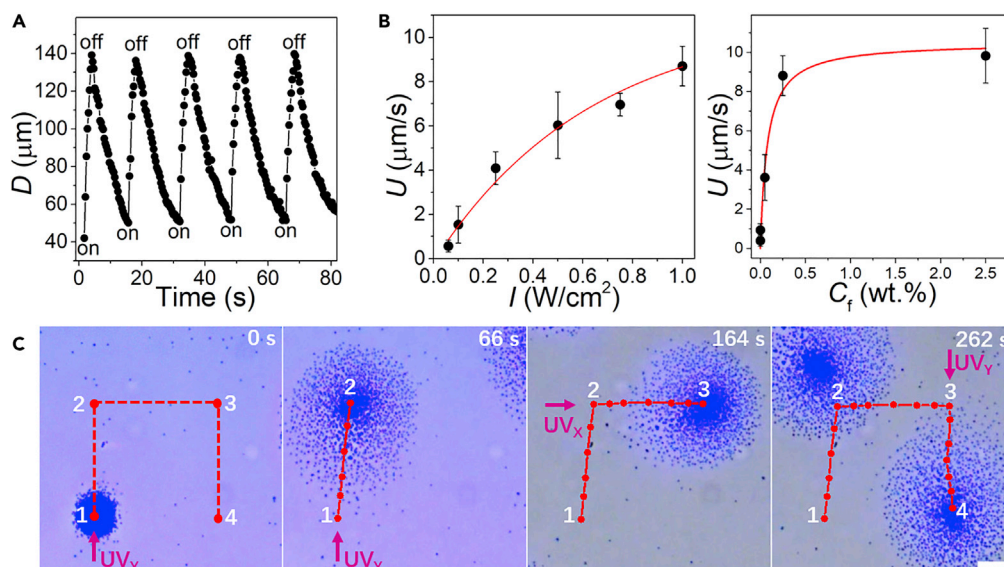


Figure 3. Light-Controlled Motions of the Flocks

(A) The size (D) versus time for a typical flock under pulsed UV_Y irradiation, indicating the reversible expansion and contraction.

(B) The velocity (U) of the micromotor flock at different UV intensity (I , left panel) and fuel concentration (C_f , right panel).

(C) The TiO_2 micromotor flock moves along a pre-designed path under the navigation of pulsed UV irradiation. Images are taken from [Video S6](#). Scale bar: 20 μm .

scattered individuals merge into 155, 88, and 44 small metastable subflocks (with an area $S_f \geq 10 \mu m^2$) in 5, 10, and 20 s, respectively, and continue to merge with prolonging time after UV is off (see [Video S7](#)). For those metastable small subflocks, if UV is turned on again at this stage, they can collectively move in a phototactic manner. For instance, one micromotor flock can split into 18 phototactic subflocks and gradually merge into four and then two subflocks before finally recovering to the original state due to the diffusiophoretic attractions with one another (the right three panels of [Figure 4A](#) and see also [Video S7](#)). The results reveal that a TiO_2 micromotor flock can reversibly split into multiple small subflocks and re-merge.

The flocking TiO_2 micromotors also show adaptive reconfigurations in response to local landscapes, such as cordon, split, re-joining, and elongation. When encountering a prism obstacle under global UV navigation, a traveling flock deforms into a V-shaped flock and embraces the obstacle, revealing the cordon reconfiguration of the micromotors ([Storms et al., 2019](#)). Then, it splits into two subflocks to adapt the profile of the obstacle when it continuously moves forward. Immediately after passing the obstacle, the two subflocks re-join at the far side of the obstacle and continue to move phototactically as a whole ([Figure 4B](#) and see also [Video S8](#)). The TiO_2 micromotor flock can also elongate its body to pass through a narrow channel as a mollusk does. When the flock moves to the inlet of a narrow channel, the micromotors in the front of the flock funnel into the open end of the channel and the micromotors near channel walls would move along them toward the open end. As a result, the flock elongates its body length to adapt the profile of the narrow channel and thereby fits through the narrow channel ([Figure 4C](#) and see also [Video S8](#)).

The adaptive reconfigurations of flocking TiO_2 micromotors to bypass obstacles can be understood by considering the different motion behaviors of individual micromotors near local landscape boundaries. Under UV irradiation, when forefront micromotors encounter impermeable and rigid walls, they can transmit the obstacle information to their neighbors or latecomers via chemical signals (i.e., O_2 molecules), of which the gradient induces the repulsive diffusiophoretic interactions with one other and the walls (see [Figure S13A](#)). The neighbors or latecomers, along with forefront micromotors, would then change their moving directions and move to the wall ends. As a result, instead of jamming at walls like single micromotors do (e.g., Wall A, see [Figure S13B](#)), the flocking micromotors can flow along walls with different directions and bypass obstacles (see [Figure S13C](#) and [Video S9](#)).

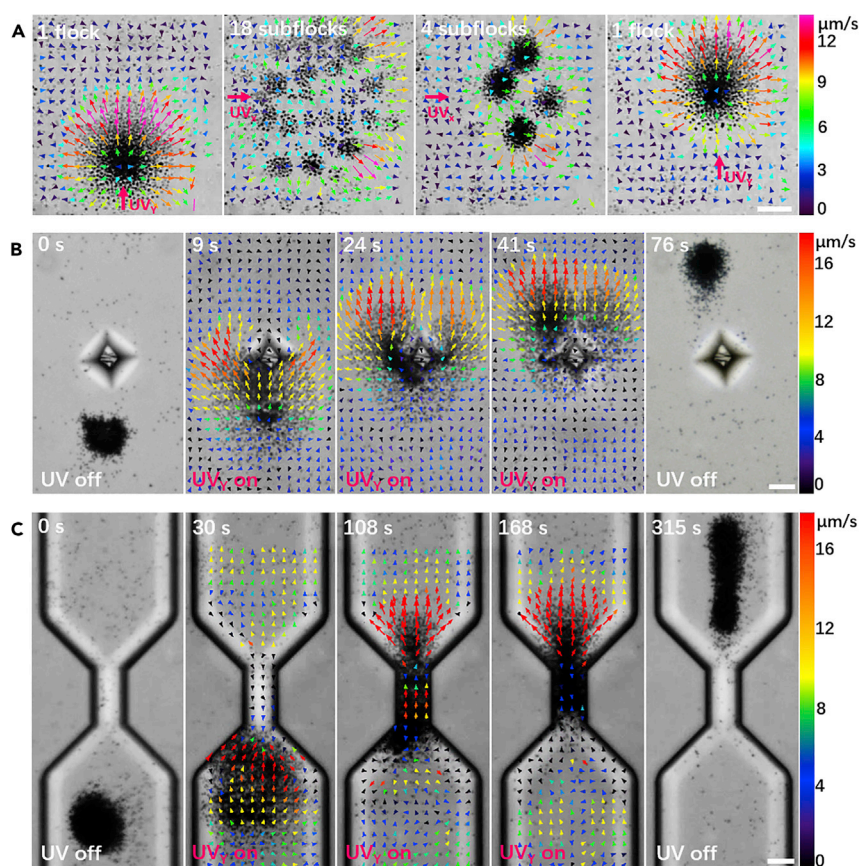


Figure 4. Adaptive Reconfigurations of the Flocks

(A) Reversible splitting and merging of the TiO_2 micromotor flock after overexpansion by regrouping the scattered individuals. Images are taken from [Video S7](#). The intensities of UV_x and UV_y are 0.25 and 1 W cm^{-2} , respectively.

(B) Cordon, splitting, and re-joining of the TiO_2 micromotor flock when it bypasses a prism obstacle.

(C) Elongation of the TiO_2 micromotor flock when it fits through a narrow channel.

Images in B and C are taken from [Video S8](#). The arrows represent the velocity vectors of the flocking micromotors. All scale bars are $20 \mu\text{m}$.

Benefitted from their collective phototaxis and adaptive reconfigurations, the flocking TiO_2 micromotors are able to perform cooperative tasks even in a complex environment. For instance, the flocking micromotors can perform cooperative cargo transport in open space and microchannels in resemblance to ants ([Feinerman et al., 2018](#)). When a flock of TiO_2 micromotors approaches a SiO_2 particle with a size of $10 \mu\text{m}$, which is ten times that the size of a single micromotor, it can load the cargo as a constituent by pulling it inward through the electrolyte diffusiophoretic attraction. Then, the micromotor flock can transport the large cargo that single motors cannot (see [Figure S14](#)) by producing a collective diffusiophoretic repulsion ([Figure 5A](#) and see also [Video S10](#)). In addition, it can also carry cargo through a microchannel by taking advantage of its adaptive reconfiguration in narrow channels ([Figure 5B](#) and see also [Video S10](#)). As the phototactic flocks are expected to load various inclusions with cooperative functions, such as other micromotors, passive particles, droplets, micro/nanodevices, cells, and microorganisms, they can be employed as a platform to create reconfigurable microrobots, active materials, and intelligent synthetic systems ([Rubenstein et al., 2014](#)). Last but not least, due to the dilatational phototactic motions of the micromotor flock, the scattering flock members can rapidly detect environmental boundaries, cover the local environment under light irradiation ([Figures 4B](#) and [4C](#)), and gather again into different collective patterns reflecting local geometrical features after the light is turned off. This implies that the micromotor flocks also have a potential for finding and mapping of local unknown environments like the macroscopic swarm robots ([Bayindir, 2016](#)), as verified by the different collective patterns when a flock embraces prism obstacles or squeezes into different narrow channels (see [Figure S15](#)).

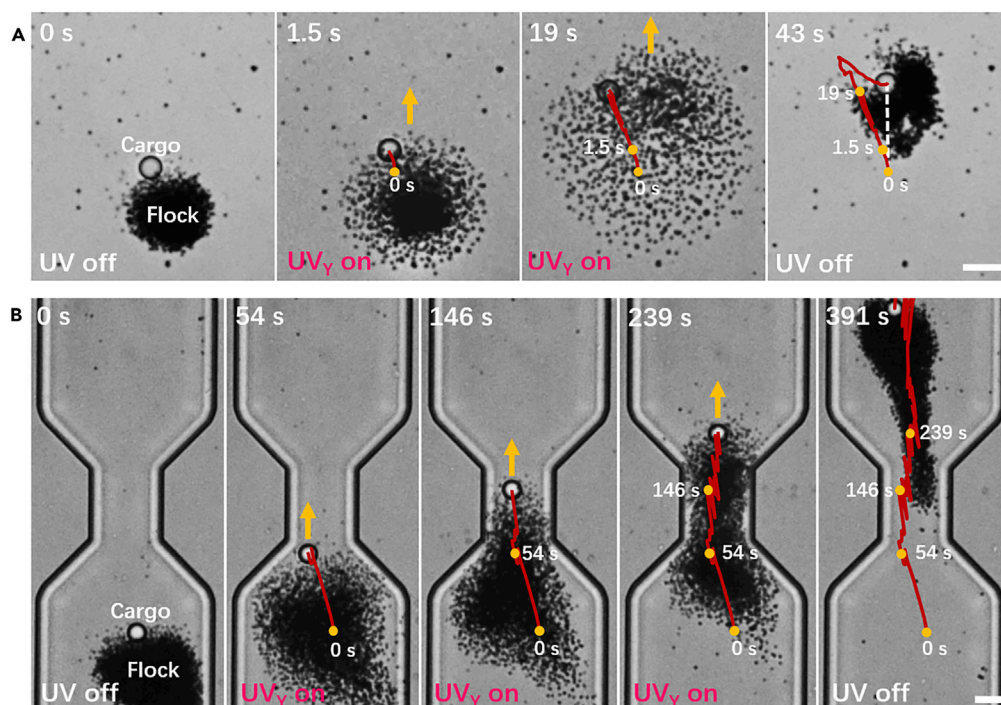


Figure 5. Cooperative Cargo Transport of the Flocking TiO₂ Micromotors

(A) A flock of TiO₂ micromotors transporting a large SiO₂ cargo (10 μm in size) in open space. The white dash line indicates the displacement of the SiO₂ cargo with the moving flock in the Y direction.

(B) A flock of TiO₂ micromotors transporting a large SiO₂ cargo (10 μm in size) in a narrow channel.

Images are taken from [Video S10](#). Golden arrows represent directions of the flocks, and red curves are trajectories of the SiO₂ cargoes. Golden dots are the positions of the cargo at different time. All scale bars are 20 μm.

DISCUSSION

In summary, we have demonstrated the phototactic flocking behaviors of TiO₂ micromotors. The TiO₂ micromotors with high hydroxyl-group content in aqueous media can spontaneously gather into flocks owing to the electrolyte diffusiophoretic attractions. Within the micromotor flocks, the individual micromotors under UV irradiation interact with one another via nonelectrolyte diffusiophoresis, and thus rich types of collective behaviors have emerged. Different from single micromotors, the flocking micromotors show a collective dilatational phototaxis with a much higher collective velocity due to the interparticle accumulation of O₂ molecules and the enhanced O₂ gradient across the flock. In addition, the micromotor flock can split into multiple subflocks by regrouping the scattered individuals, and it also exhibits adaptive group reconfigurations according to local landscapes due to the different behaviors of individuals near the landscape boundaries. Therefore, the micromotor flocks under the pulsed light navigation can migrate along pre-designed paths and bypass obstacles. Moreover, owing to the enhanced driving force and rapid dilatational area covering, they can execute cooperative tasks that single micromotors cannot achieve, such as cooperatively transporting cargoes significantly larger than the single micromotor and also collectively mapping local microenvironments. The as-developed photochemical micromotor flocks are expected to inspire the creation of reconfigurable microrobots, active materials, and intelligent synthetic systems.

Limitations of the Study

As the collective behaviors of the hydroxyl-rich TiO₂ micromotors are strongly dependent on their local diffusiophoretic interactions, their primary limitation is the sensitivity to ion concentrations. This limitation makes them difficult to operate in biological media, such as simulated body fluid, serum, or whole blood. Nonetheless, this study has demonstrated that the flocking TiO₂ micromotors are powerful for executing cooperative tasks in a deionized water environment due to their intriguing collective behaviors, such as cooperative large-cargo transport and collective microenvironment mapping.

METHODS

All methods can be found in the accompanying [Transparent Methods](#) supplemental file.

SUPPLEMENTAL INFORMATION

Supplemental Information can be found online at <https://doi.org/10.1016/j.isci.2019.07.050>.

ACKNOWLEDGMENTS

This work was supported by the National Natural Science Foundation of China (21875175, 21474078, 51521001, 11574222 and 21522404), the Top Talents Lead Cultivation Project and Natural Science Foundation of Hubei Province (2015CFA003), and the Priority Academic Program Development of Jiangsu Higher Education Institutions. We acknowledge Prof. Haihang Cui from Xi'an University of Architecture and Technology for his valuable discussion related to the numerical simulation. We also acknowledge Mr. Xiaofeng Li and Mr. Ming You for their valuable discussion and the revision of the manuscript.

AUTHOR CONTRIBUTIONS

F.M. and J.G. conceived the idea and designed the study. J.Z., F.M., and Z.W. performed the experiments. F.M., Z.Z., and S.D. performed the simulations. F.M., J.Z., Z.Z., and J.G. analyzed the data and co-wrote the manuscript. F.M. and J.G. initiated and supervised the project. All the authors contributed to the discussion and reviewed the manuscript.

DECLARATION OF INTERESTS

The authors declare no competing interests.

Received: June 18, 2019

Revised: July 24, 2019

Accepted: July 30, 2019

Published: September 27, 2019

REFERENCES

- Anderson, J.L. (1989). Colloid transport by interfacial forces. *Annu. Rev. Fluid Mech.* **21**, 61–99.
- Aranson, I.S., and Sapozhnikov, M.V. (2004). Theory of pattern formation of metallic microparticles in poorly conducting liquids. *Phys. Rev. Lett.* **92**, 234301.
- Attanasi, A., Cavagna, A., Del Castello, L., Giardina, I., Melillo, S., Parisi, L., Pohl, O., Rossaro, B., Shen, E., Silvestri, E., et al. (2014). Collective behaviour without collective order in wild swarms of midges. *PLOS Comput. Biol.* **10**, e1003697.
- Bayindir, L. (2016). A review of swarm robotics tasks. *Neurocomputing* **172**, 292–321.
- Boehm, H.P. (1971). Acidic and basic properties of hydroxylated metal oxide surfaces. *Discuss. Faraday Soc.* **52**, 264–275.
- Chen, C., Liu, S., Shi, X.Q., Chate, H., and Wu, Y.L. (2017a). Weak synchronization and large-scale collective oscillation in dense bacterial suspensions. *Nature* **542**, 210–214.
- Chen, C., Mou, F., Xu, L., Wang, S., Guan, J., Feng, Z., Wang, Q., Kong, L., Li, W., Wang, J., et al. (2017b). Light-steered isotropic semiconductor micromotors. *Adv. Mater.* **29**, 1603374.
- Deng, Z., Mou, F., Tang, S., Xu, L., Luo, M., and Guan, J. (2018). Swarming and collective migration of micromotors under near infrared light. *Appl. Mater. Today* **73**, 45–53.
- Duan, W., Liu, R., and Sen, A. (2013). Transition between collective behaviors of micromotors in response to different stimuli. *J. Am. Chem. Soc.* **135**, 1280–1283.
- Feinerman, O., Pinkoviezky, I., Gelblum, A., Fonio, E., and Gov, N.S. (2018). The physics of cooperative transport in groups of ants. *Nat. Phys.* **14**, 683–693.
- Guix, M., Mayorga-Martinez, C.C., and Merkoçi, A. (2014). Nano/micromotors in (bio)chemical science applications. *Chem. Rev.* **114**, 6285–6322.
- Gun'ko, V.M., Zarko, V.I., Lebeda, R., and Chibowski, E. (2001). Aqueous suspension of fumed oxides: particle size distribution and zeta potential. *Adv. Colloid Interface* **91**, 1–112.
- Hong, Y.Y., Diaz, M., Cordova-Figueroa, U.M., and Sen, A. (2010). Light-driven titanium-dioxide-based reversible microfireworks and micromotor/micropump systems. *Adv. Funct. Mater.* **20**, 1568–1576.
- Ibele, M., Mallouk, T.E., and Sen, A. (2009). Schooling behavior of light-powered autonomous micromotors in water. *Angew. Chem. Int. Ed.* **48**, 3308–3312.
- Ioannou, C.C., Guttal, V., and Couzin, I.D. (2012). Predatory fish select for coordinated collective motion in virtual prey. *Science* **337**, 1212–1215.
- Li, J., Rozen, I., and Wang, J. (2016). Rocket science at the nanoscale. *ACS Nano* **10**, 5619–5634.
- Litvak, M.K. (1993). Response of shoaling fish to the threat of aerial predation. *Environ. Biol. Fish.* **36**, 183–192.
- Moran, J.L., and Posner, J.D. (2017). Phoretic self-propulsion. *Annu. Rev. Fluid Mech.* **49**, 511–540.
- Mou, F., Li, Y., Chen, C., Li, W., Yin, Y., Ma, H., and Guan, J. (2015). Single-component TiO₂ tubular microengines with motion controlled by light-induced bubbles. *Small* **11**, 2564–2570.
- Palacci, J., Sacanna, S., Steinberg, A.P., Pine, D.J., and Chaikin, P.M. (2013). Living crystals of light-activated colloidal surfers. *Science* **339**, 936–940.
- Parrish, J.K., and Edelstein-Keshet, L. (1999). Complexity, pattern, and evolutionary trade-offs in animal aggregation. *Science* **284**, 99–101.
- Reynolds, C.W. (1987). Flocks, herds and schools: a distributed behavioral model. *ACM SIGGRAPH Comput. Graph.* **21**, 25–34.
- Rubenstein, M., Cornejo, A., and Nagpal, R. (2014). Programmable self-assembly in a thousand-robot swarm. *Science* **345**, 795–799.

- Sánchez, S., Soler, L., and Katuri, J. (2015). Chemically powered micro- and nanomotors. *Angew. Chem. Int. Ed.* 54, 1414–1444.
- Sapozhnikov, M.V., Tolmachev, Y.V., Aranson, I.S., and Kwok, W.K. (2003). Dynamic self-assembly and patterns in electrostatically driven granular media. *Phys. Rev. Lett.* 90, 114301.
- Schaerf, T.M., Dillingham, P.W., and Ward, A.J.W. (2017). The effects of external cues on individual and collective behavior of shoaling fish. *Sci. Adv.* 3, e1603201.
- Singh, D.P., Choudhury, U., Fischer, P., and Mark, A.G. (2017). Non-equilibrium assembly of light-activated colloidal mixtures. *Adv. Mater.* 29, 1701328.
- Solovev, A.A., Sanchez, S., Pumera, M., Mei, Y.F., and Schmidt, O.G. (2010). Magnetic control of tubular catalytic microbots for the transport, assembly, and delivery of micro-objects. *Adv. Funct. Mater.* 20, 2430–2435.
- Storms, R.F., Carere, C., Zoratto, F., and Hemelrijk, C.K. (2019). Complex patterns of collective escape in starling flocks under predation. *Behav. Ecol. Sociobiol.* 73, 10.
- Sugimoto, T., and Zhou, X. (2002). Synthesis of uniform anatase TiO₂ nanoparticles by the gel-sol method. *J. Colloid Interface Sci.* 252, 347–353.
- Vicsek, T., and Zafeiris, A. (2012). Collective motion. *Phys. Rep.* 517, 71–140.
- Wang, H., and Pumera, M. (2015). Fabrication of micro/nanoscale motors. *Chem. Rev.* 115, 8704–8735.
- Wang, W., Duan, W., Ahmed, S., Sen, A., and Mallouk, T.E. (2015). From one to many: dynamic assembly and collective behavior of self-propelled colloidal motors. *Acc. Chem. Res.* 48, 1938–1946.
- Wu, C.-Y., Tu, K.-J., Lo, Y.-S., Pang, Y.L., and Wu, C.-H. (2016). Alkaline hydrogen peroxide treatment for TiO₂ nanoparticles with superior water-dispersibility and visible-light photocatalytic activity. *Mater. Chem. Phys.* 181, 82–89.
- Wu, Z.G., Troll, J., Jeong, H.H., Wei, Q., Stang, M., Ziemssen, F., Wang, Z.G., Dong, M.D., Schnichels, S., Qiu, T., et al. (2018). A swarm of slippery micropropellers penetrates the vitreous body of the eye. *Sci. Adv.* 4, eaat4388.
- Xie, H., Sun, M., Fan, X., Lin, Z., Chen, W., Wang, L., Dong, L., and He, Q. (2019). Reconfigurable magnetic microrobot swarm: Multimode transformation, locomotion, and manipulation. *Sci. Robot.* 4, eaav8006.
- Xu, L., Mou, F., Gong, H., Luo, M., and Guan, J. (2017). Light-driven micro/nanomotors: from fundamentals to applications. *Chem. Soc. Rev.* 46, 6905–6926.
- Xu, T., Soto, F., Gao, W., Dong, R., Garcia-Gradilla, V., Magaña, E., Zhang, X., and Wang, J. (2015). Reversible swarming and separation of self-propelled chemically powered nanomotors under acoustic fields. *J. Am. Chem. Soc.* 137, 2163–2166.
- Xu, T.L., Soto, F., Gao, W., Garcia-Gradilla, V., Li, J.X., Zhang, X.J., and Wang, J. (2014). Ultrasound-modulated bubble propulsion of chemically powered microengines. *J. Am. Chem. Soc.* 136, 8552–8555.
- Yan, J., Han, M., Zhang, J., Xu, C., Luijten, E., and Granick, S. (2016). Reconfiguring active particles by electrostatic imbalance. *Nat. Mater.* 15, 1095–1099.
- You, M., Chen, C., Xu, L., Mou, F., and Guan, J. (2018). Intelligent micro/nanomotors with Taxis. *Acc. Chem. Res.* 51, 3006–3014.
- Yu, J., Wang, B., Du, X., Wang, Q., and Zhang, L. (2018). Ultra-extensible ribbon-like magnetic microswarm. *Nat. Commun.* 9, 3260.
- Zottl, A., and Stark, H. (2016). Emergent behavior in active colloids. *J. Phys. Condens. Matter* 28, 253001.

ISCI, Volume 19

Supplemental Information

Phototactic Flocking of Photochemical Micromotors

Fangzhi Mou, Jianhua Zhang, Zhen Wu, Sinan Du, Zexin Zhang, Leilei Xu, and Jianguo Guan

Supplemental Figures

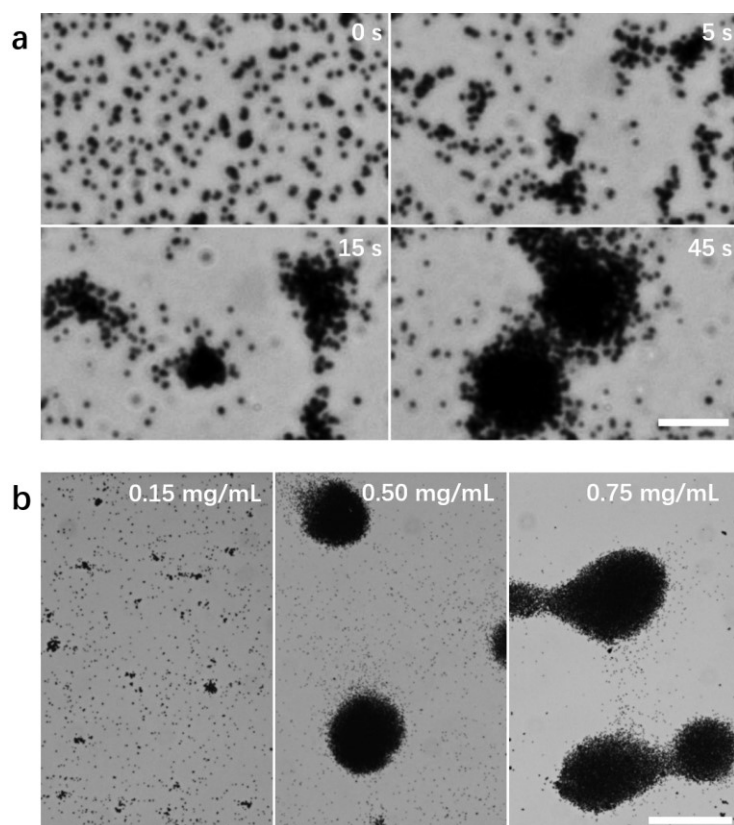


Figure S1. The clustering behaviors of the dispersed TiO₂ micromotors. (a) The clustering process of the TiO₂ micromotors over time. Images are taken from Video S1. Scale bar: 20 μm . Well-dispersed particles would gather into small flocks at first, and then they further grow into large flocks by absorbing neighboring particles or small flocks. (b) The formed TiO₂ micromotor flocks at different Cp of 0.15, 0.5 and 0.75 mg/ml in water with 0.25 wt.% H₂O₂. Scale bar: 100 μm . Related to Figure 1.

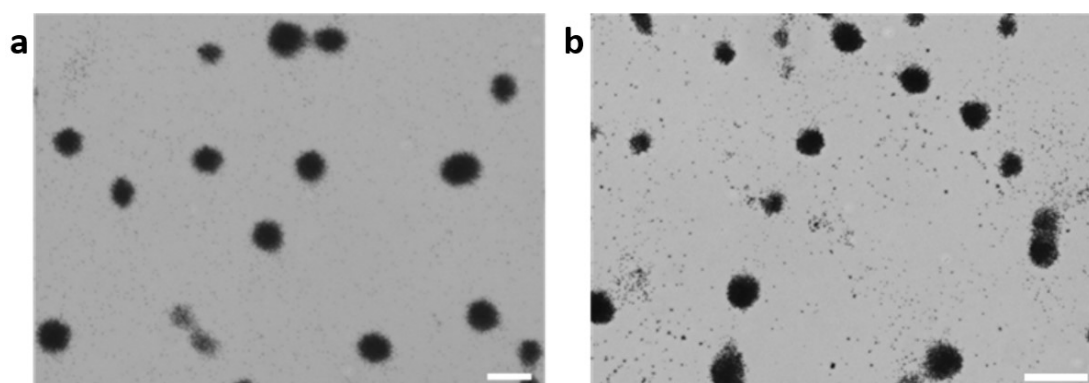


Figure S2. Flocks formed in pure water under natural light and in dark. (a) The flocks of TiO₂ micromotors formed in pure water. (b) The flocks of TiO₂ micromotors formed in 0.25 wt.% H₂O₂ solution in dark. Scale bars: 50 μm . Related to Figure 1.

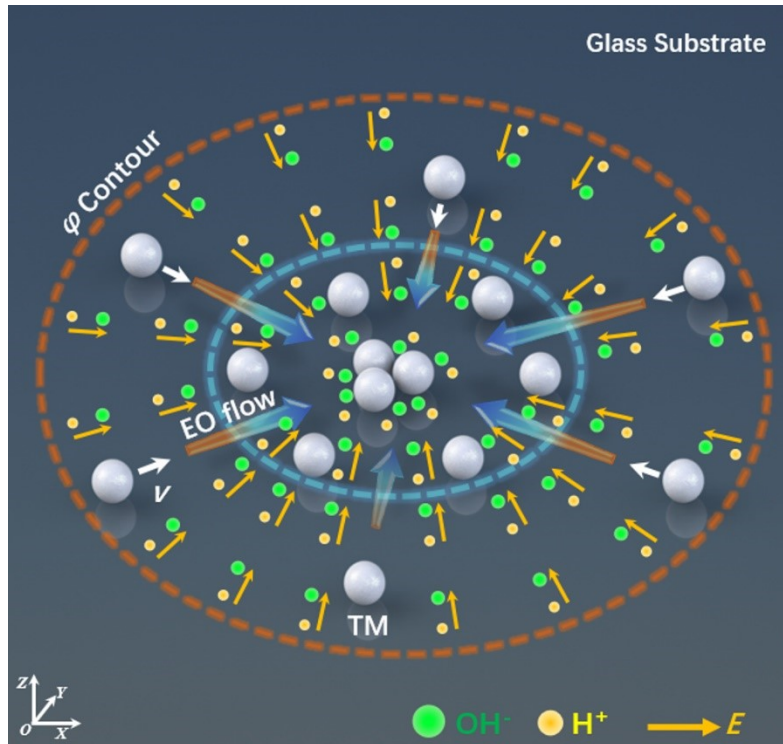


Figure S3. Clustering mechanism. The schematic illustration of the clustering of TiO_2 micromotors (TM) along with the electroosmotic flow (EO flow) under electrolyte diffusiophoresis. Related to Figure 1.

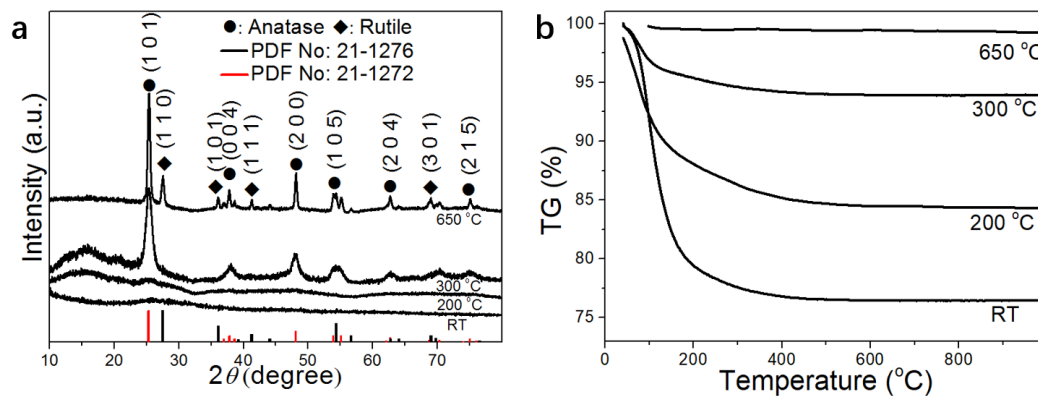


Figure S4. Characterization of TiO_2 micromotors obtained at different temperature. (a) XRD patterns and (b) TG analysis of the TiO_2 micromotors before calcination (RT) and those calcined at 200, 300 and 650 °C, respectively. Related to Figure 1.

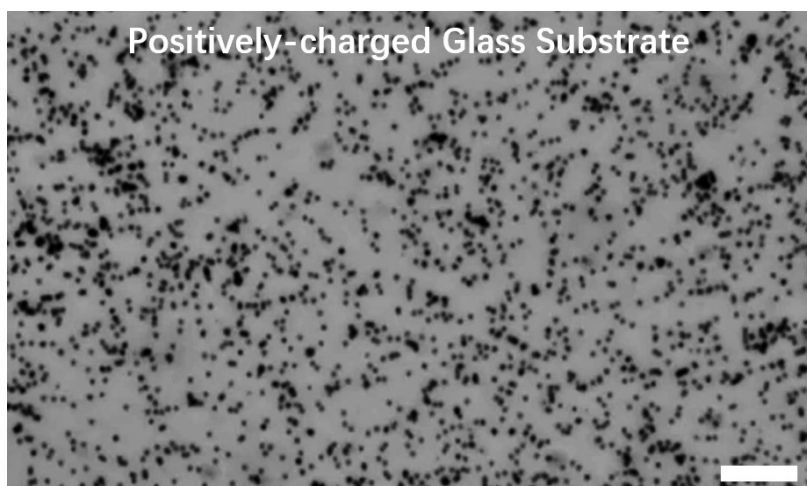


Figure S5. The TiO₂ micromotors on a positively-charged glass substrate in the medium. Scale bar: 50 μm . Related to Figure 1.

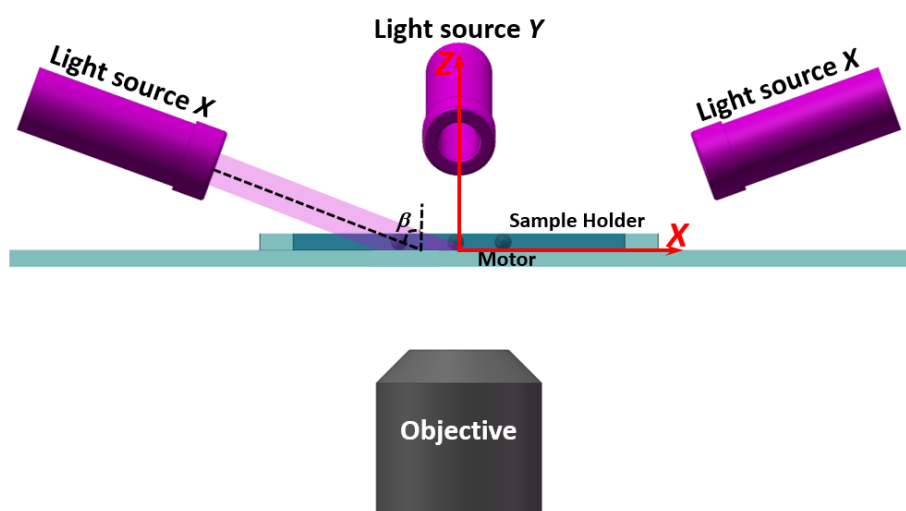


Figure S6. Schematic diagram of the experimental setup for the light irradiation. The coordinate is set up as demonstrated, Y axis points into the screen, light irradiators X and Y control the motion at X, Y directions respectively. For the convenience of operation, the light sources were set up to have an angle β with Z axis. Related to Figure 2.

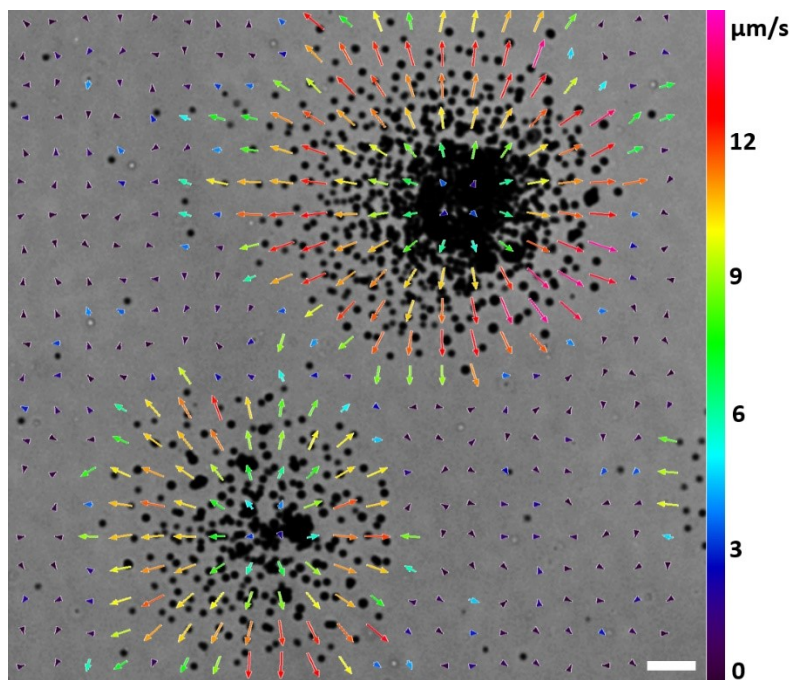


Figure S7. Instantaneous velocity vectors of the TiO_2 micromotors in two flocks under UV_z irradiation. Related to Figure 2.

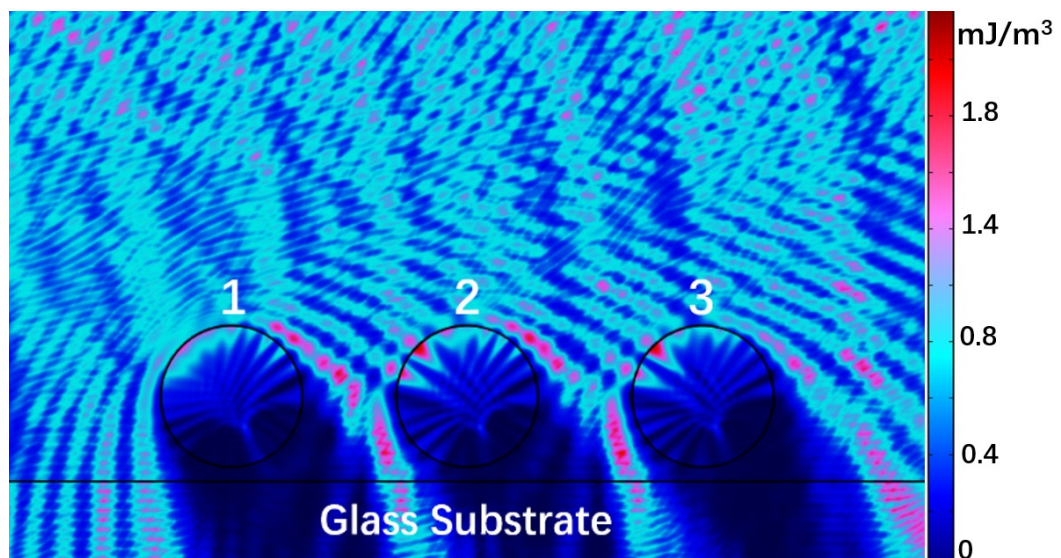


Figure S8. Numerical simulation of light intensity in micromotors. The simulated time-averaged light energy density in TiO_2 micromotor 1, 2 and 3 with an interparticle distance of $3 \mu\text{m}$. Related to Figure 2.

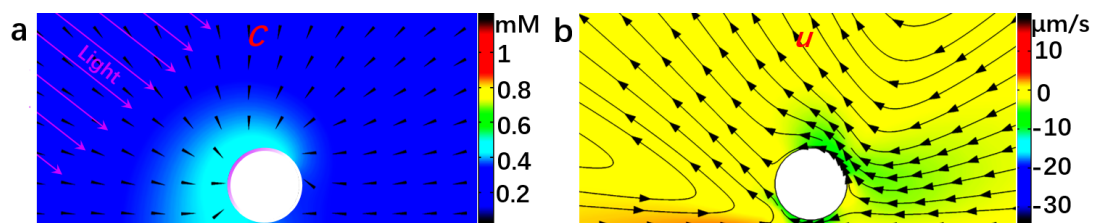


Figure S9. (a) Steady-state distribution of O_2 concentration (C) around a TiO_2 micromotor, in which the black triangles represent the gradient (∇C) of O_2 concentration. Purple arrows and curves represent the direction of incident UV light and the illuminated surfaces of the micromotors, respectively. (b) The simulated velocity in the X direction (u) and the streamlines (black curves) of the hydrodynamic flow induced by ∇C along the surface of the particles. Related to Figure 2.

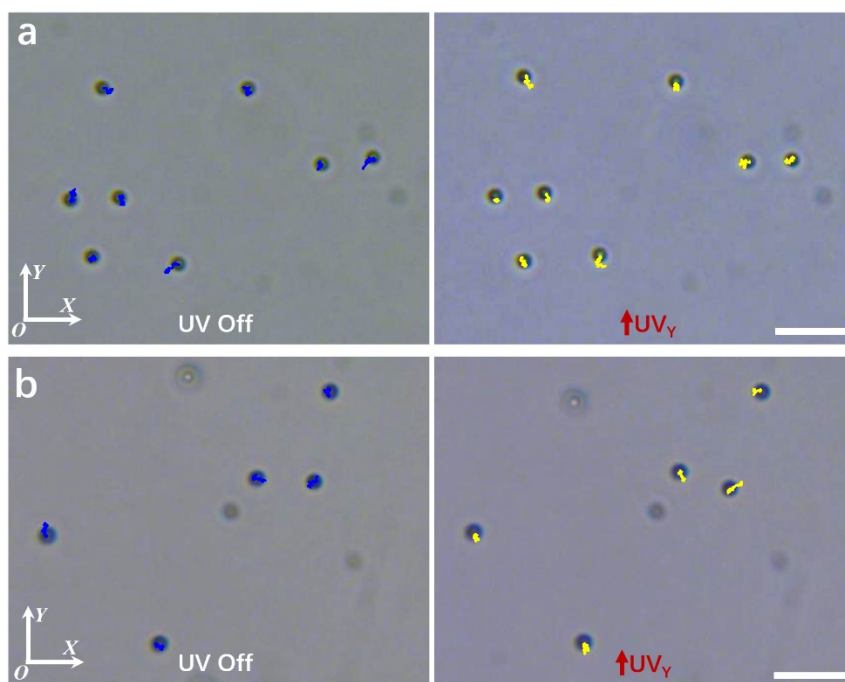


Figure S10. The motions of the passive (a) SiO_2 and (b) PS microparticles when UV_y is off and on, respectively. Images are taken from Video S5. Scale bar: $10 \mu m$. Related to Figure 2.

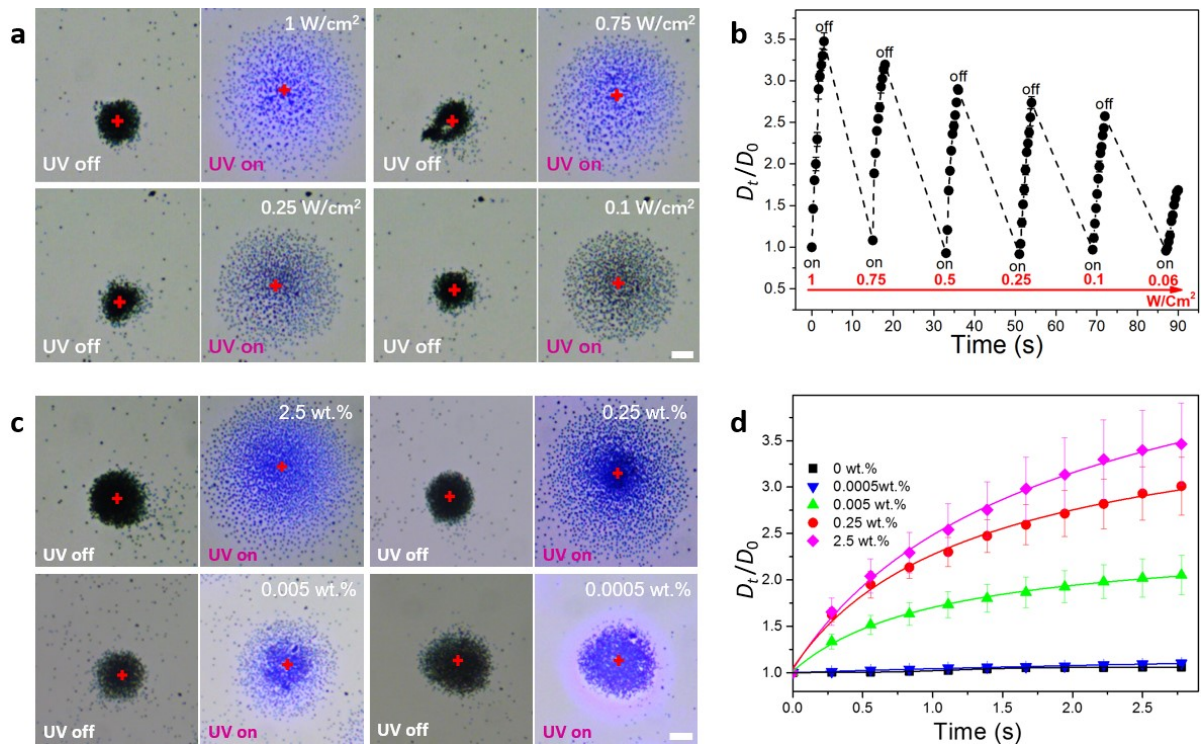


Figure S11. Phototaxis of the micromotor flocks at different UV intensity and fuel concentration. (a) Representative snapshots of the micromotor flock without and with UV irradiation at different light intensities, and (b) the normalized size (D_t/D_0) variation of the flock at different light intensities. (c) Representative snapshots of the micromotor flock without and with UV irradiation at different fuel concentration, and (d) the corresponding D_t/D_0 versus irradiation time. Scale bars: 20 μm . Related to Figure 3.

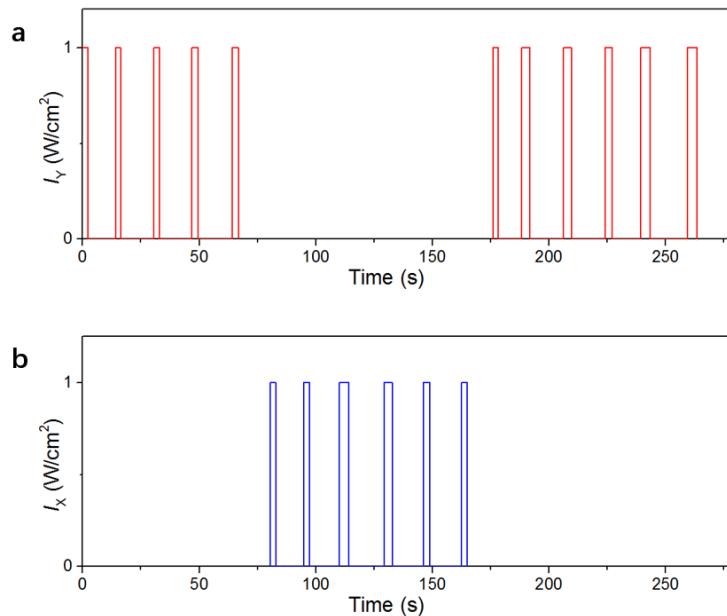


Figure S12. The on-off repeating cycles of UV irradiation. (a) The on-off repeating cycles of UV_Y for the navigation of the phototactic flock in the Y direction. (b) The on-off repeating cycles of UV_X for the navigation of the phototactic flock in the X direction. Related to Figure 3.

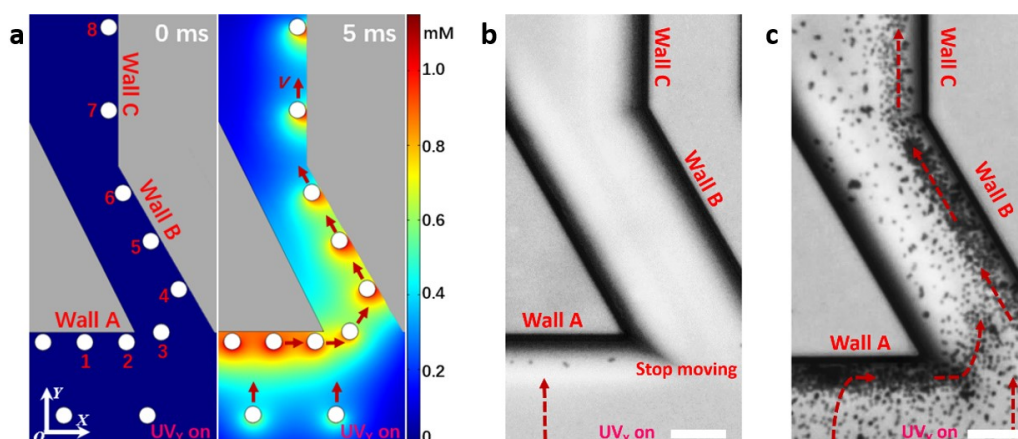


Figure S13. Interactions between individual micromotors and obstacle walls. (a) Numerical simulation of the distribution of the photocatalytically generated O_2 around the micromotors near obstacle walls with different angles (ϑ) to their phototactic motion axis (Y direction). Interacting micromotors could easily move along Wall A ($\vartheta = 90^\circ$), Wall B ($\vartheta = 60^\circ$) and Wall C ($\vartheta = 0^\circ$) due to the desired O_2 gradient across the micromotors (Micromotor 1-8) along the walls. (b) The trapped single motors near Wall A under UV_V irradiation. (c) The flocking of the micromotors along obstacle walls under UV_V irradiation. Scale bars: 20 μm . Related to Figure 4.

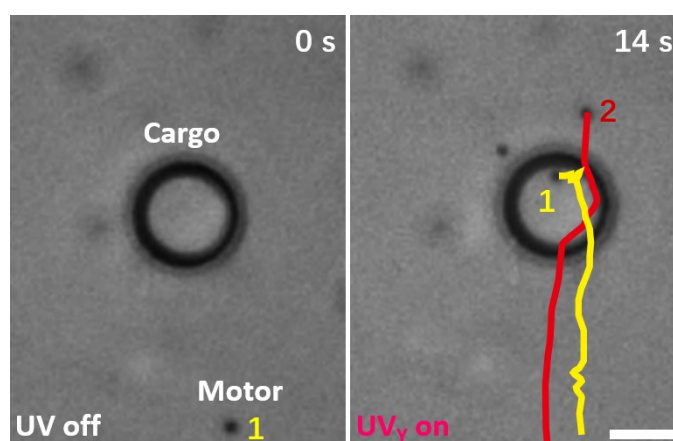


Figure S14. Cargo transport by single micromotors. Time-lapse optical microscopic images showing that single TiO_2 micromotors (motor 1 and 2) fail to move a large cargo (10 μm in size) due to its small size and weak driving forces. Yellow and red curves are trajectories of motor 1 and 2 under UV irradiation, respectively. Scale bar: 5 μm . Related to Figure 5.

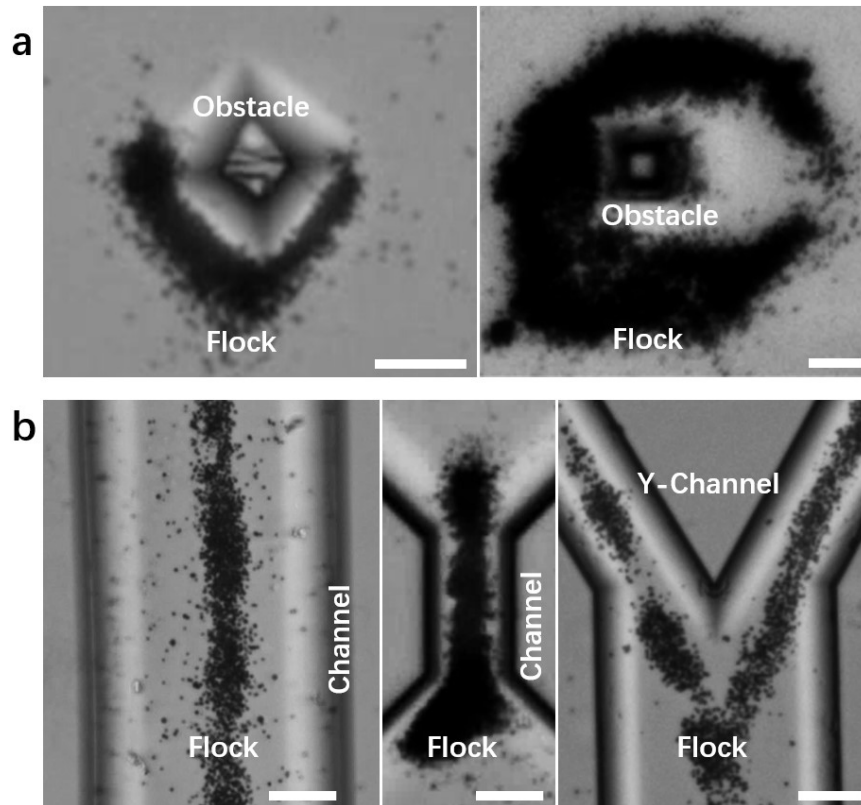


Figure S15. Collective patterns of the micromotor flocks in local microenvironments. (a) V-shaped and C-shaped flocks are formed if they embrace rhombus and square obstacles, respectively. (b) Wire-like, dumbbell, and Y-shaped micromotor flocks are formed in straight, flared and Y-shaped microchannels, respectively. Scale bars: 20 μm . Related to Figure 4.

Transparent Methods

Synthesis of TiO₂ micromotors. Spherical anatase TiO₂ microparticles with rich hydroxyl groups were fabricated as individual micromotors (Chen et al., 2017b). At first, the hydrous TiO₂ microparticles with a diameter of 1.2 μm were synthesized referring to the previous method. Then, the hydrous TiO₂ microparticles were calcined at 300 °C for 2 h to crystallize the microparticles while maintaining their high C_{OH}. Anatase TiO₂ microparticles with different C_{OH} were also fabricated by calcining the hydrous TiO₂ microparticles at 200 and 650 °C for 2 h, respectively. Those microparticles obtained at 650 °C were further treated by the alkaline hydrogen peroxide solution with 8 M NaOH and 0.1 M H₂O₂ to increase their C_{OH} (Wu et al., 2016).

Characterization. Scanning electron microscopy (SEM) images were obtained by Hitachi S-4800 Field-emission SEM (Japan). The Zeta potential of the micromotors was measured by Malvern Zetasizer Nano Z (Britain). The X-ray diffraction (XRD) patterns of the samples were recorded using a Rigaku D/Max-2000 diffractometer equipped with a Cu K radiation source ($\lambda=0.15418$ nm). Thermogravimetry-differential scanning calorimeter (TG-DSC) analysis was carried out on a NETZSEC STA-449C thermal analyzer (Germany). The quantitative elementary analysis of hydrogen was measured by CHNS/O element analyzer (Vario EL cube, Germany). The hydroxyl group content in the TiO₂ micromotors is calculated from the curves of TG weight loss and quantitative elementary analysis.

Spontaneous clustering and phototactic flocking of the TiO₂ micromotors. A 100 μL suspension of the TiO₂ micromotors was dropped onto a glass slide (Citotest 1A5107), followed by adding 100 μL of the 0.5 wt.% H₂O₂ fuel solution. The concentration of the micromotors in the suspension was adjusted to 0.15, 0.35, 0.5 and 0.75 mg ml⁻¹ to observe their clustering behaviors, respectively. Clustering behaviors of the micromotors in the medium without H₂O₂, in dark and on a positive-charge modified glass slide (Citoglas 188105W) were also investigated. Four lamps with a wavelength of 365 nm (SZ Lamplic Technology) were set above the substrate along with two orthogonal directions (see Figure S6), the incident angles (θ) were set to be 45°. The four UV lamps (SZ Lamplic Technology, China) with maximum I of 1 W cm⁻² were switched on and off serially according to the pre-designed program. The motions of the micromotor flock under the navigation of light were observed and recorded at room temperature by an inverted optical microscope (Leica DMI 3000 M). Videos were analyzed by using ImageJ and Video Spot Tracker Vo8.01 software. The velocity of the flock was determined by calculating the displacement of centroid of flocks per second under light irradiation.

Particle image velocimetry analysis. The velocity field of the micromotor flocks was quantitatively determined by micro-particle imaging velocimetry (μ PIV) (Lindken et al., 2009), which provides velocity data at the micrometer scale. Here the μ PIV analysis was performed using an in-house computer program written in Interactive Data Language (IDL, Exelis Visual Information Solutions). Briefly, two sequential digital images were taken by a bright-field microscope. The images were divided into small regions as interrogation windows, and then the local mean displacement of each point contained in the interrogation window was calculated by a two-dimensional cross-correlation algorithm. The corresponding velocity of each point was calculated by dividing the displacement vector by the time interval between the two images. Unlike conventional PIV measure where tracer particles are added for the visualization of motions, here the micromotors themselves act as tracers.

Quantitative Detection of the flux of O₂ molecules from TiO₂ micromotors. A 10 mL aqueous suspension of TiO₂ micromotors (0.07 mg mL⁻¹) and H₂O₂ (0.25 wt.%) was put into a 10 mL beaker mounted with the probe of dissolved oxygen meter (Jenco 9173R, USA). A UV-LED light source (SZ Lamplic Technology, China) with a wavelength of 365 nm was set below the beaker. The concentration of the dissolved oxygen was measured when the UV light ($I = 1$ W cm⁻²) was

turning on and off repeatedly. The concentration of the dissolved oxygen in a solution only with H₂O₂ (0.25 wt.%) was also measured by taking the same procedures. The flux of O₂ molecules (J_{O_2}) from the illuminated surface of the micromotors was calculated according to the following equation.

$$J_{O_2} = \frac{C_t - C_0}{NS_p t} = \frac{2\pi r \rho (C_t - C_0)}{3C_p V t}$$

Here, C_0 is the concentration of the dissolved oxygen in the aqueous suspension before UV irradiation, and C_t is that at time of t under UV irradiation, in which C_t is obtained by deducting the increased O₂ concentration at t of the H₂O₂ (0.25 wt.%) solution under UV irradiation. N is the number of TiO₂ micromotors in unit volume. S_p and r are the surface area and radius of a TiO₂ micromotor. C_p is the concentration of TiO₂ micromotors in the aqueous suspension, and V is the volume of the aqueous suspension.

Numerical simulation.

a. Governing equations

Electrolyte diffusiophoretic interactions between TiO₂ micromotors

When the TiO₂ micromotors with rich hydroxyl groups are dispersed in water, they simultaneously secrete H⁺ ions from surface acidic bridging hydroxyls ($pK_a = 2.9$) and OH⁻ ions from basic terminal hydroxyls ($pK_b = 1.3$), respectively. The distribution of H⁺ and OH⁻ is determined by the ion flux (J_i), diffusion, convection and migration of ions (Equation 1), and it is solved with the conservation equation (Equation 2) at steady state.

$$J_i = \mathbf{u}c_i - D_i \nabla c_i - \frac{z_i F D_i c_i \nabla \varphi}{RT} \quad (1)$$

$$\nabla \cdot J_i = 0 = \mathbf{u} \cdot \nabla c_i - D_i \nabla^2 c_i - \frac{z_i F D_i \nabla \cdot (c_i \nabla \varphi)}{RT} \quad (2)$$

Where \mathbf{u} is the fluid velocity, F is the Faraday constant, φ is the electrostatic potential, R is the gas constant, T is the absolute temperature, and c_i , D_i , z_i are the concentration, diffusion coefficient, and charge of species i (H⁺ or OH⁻), respectively.

The electric potential (φ) in Equation 1 is calculated using the Poisson equation,

$$-\varepsilon_0 \varepsilon_r \nabla^2 \varphi = \rho_e = F(z_+ c_+ + z_- c_-) \quad (3)$$

where ρ_e is the volumetric charge density, z_+ and z_- are the charges of the cations and the anions, c_+ and c_- are the concentrations of the cations and the anions, ε_0 is the permittivity of the vacuum, and ε_r is the relative permittivity of the fluid media, respectively.

The inertial effect is neglected in the present study because of a very small Reynolds number. Thus, the flow field is governed by the Stokes equations,

$$-\nabla p + \mu \nabla^2 \mathbf{u} = 0 \quad (4)$$

and the continuity equation for the incompressible fluid,

$$\nabla \cdot \mathbf{u} = 0 \quad (5)$$

In these equations, \mathbf{u} is the fluid velocity vector, and p is the pressure. The initial values of the flow velocity and the pressure are all zero. The electroosmotic flow boundary conditions are as following:

$$\text{On the particle surface, } \mathbf{u} = \frac{\varepsilon_0 \varepsilon_r \zeta_p}{\mu} (\mathbf{I} - \mathbf{nn}) \cdot \nabla \varphi \quad (6)$$

$$\text{On the substrate surface, } \mathbf{u} = \frac{\varepsilon_0 \varepsilon_r \zeta_w}{\mu} (\mathbf{I} - \mathbf{nn}) \cdot \nabla \varphi \quad (7)$$

In these equations, ζ_p and ζ_w are the Zeta potential of the TiO₂ micromotors and the wall (glass substrate), respectively. The quantity $(\mathbf{I} - \mathbf{nn})$ defines the electric field tangential to the charged surface, with \mathbf{I} denoting the second-order unit tensor.

Nonelectrolyte diffusiophoretic interactions between TiO₂ micromotors under UV irradiation

Under UV irradiation, a flux of O₂ molecules is induced on the illuminated surfaces of the TiO₂ micromotors due to the

photocatalytic decomposition of H_2O_2 . The distribution of O_2 molecules is governed by the O_2 flux (J_{O_2}), diffusion and convection (Equation 8), and it is solved with the conservation equation (Equation 9) at steady state.

$$J_{\text{O}_2} = \mathbf{u}c_{\text{O}_2} - D_{\text{O}_2}\nabla c_{\text{O}_2} \quad (8)$$

$$\nabla \cdot J_{\text{O}_2} = 0 = \mathbf{u} \cdot \nabla c_{\text{O}_2} - D_{\text{O}_2}\nabla^2 c_{\text{O}_2} \quad (9)$$

Where c_{O_2} and D_{O_2} are the concentration and diffusion coefficient of O_2 molecules in water, respectively. Also, the inertial effect is neglected, the fluid is considered to be incompressible, and initial values of the flow velocity and the pressure are all zero in the present study. The boundary conditions of the chemiosmotic slip are as following:

$$\text{On the particle surface, } \mathbf{u} = -b_p(\mathbf{I} - \mathbf{nn}) \cdot \nabla c_{\text{O}_2} \quad (10)$$

$$\text{On the substrate surface, } \mathbf{u} = -b_w(\mathbf{I} - \mathbf{nn}) \cdot \nabla c_{\text{O}_2} \quad (11)$$

In these equations, b_p and b_w are surface mobility of the TiO_2 micromotors and the glass substrate that encapsulate the molecular details of the interaction between the solute (O_2 molecules) and the surface.

b. Parameter setting in COMSOL model

The simulations were performed by using diffusions, electrostatics and creeping flow modules of COMSOL Multiphysics software. For the numerical simulation of the local E generated by the different diffusivities of the secreted H^+ and OH^- and the electroosmotic flow induced by E , the simulation model is built up by placing three TiO_2 micromotors on a glass substrate (100 μm in width), which is immersed in the bottom of 0.01 mm^2 square space which is filled with water. The release rate and diffusion coefficients (D) of H^+ and OH^- are set to be $8.90 \times 10^{-8} \text{mol m}^{-2} \cdot \text{s}^{-1}$, $9.31 \times 10^{-9} \text{m}^2 \text{s}^{-1}$ and $5.27 \times 10^{-9} \text{m}^2 \text{s}^{-1}$, respectively (Jang et al., 2016). Zeta potential (ζ) of the TiO_2 micromotors was measured to be -17 mV, and that of the glass substrate was set to be -85 mV (Duan et al., 2013), respectively. The bulk proton concentration was set to be $2.24 \times 10^{-3} \text{mol m}^{-3}$, the value for saturated water with ambient CO_2 at pH 5.65 (Jang et al., 2016). For the numerical simulation of the asymmetric O_2 concentration (C) distribution and chemiosmotic flow around three TiO_2 micromotors with an interparticle distance of 2 μm , and the flux (J_{O_2}) of O_2 molecules from the illuminated surface of the TiO_2 micromotor due to the photocatalytic H_2O_2 decomposition was measured to be $4.13 \times 10^{-4} \text{mol m}^{-2} \text{s}^{-1}$. The surface mobility over the particle surface (b_p) is deduced to be $8.50 \times 10^{-11} \text{m}^5 \text{mol}^{-1} \text{s}^{-1}$ by parameter sweep in the simulation of the chemiosmotic flow velocity in X -axis (u) at the surface according to J_{O_2} and v ($4.5 \mu\text{m s}^{-1}$) of a single TiO_2 particle, and surface mobility over the substrate surface (b_w) is set to be $0.5b_p$ (Singh et al., 2018). The diffusion coefficient of O_2 molecules in water is $1.97 \times 10^{-9} \text{m}^2 \text{s}^{-1}$ (Chen et al., 2017b).

Supplemental References

Jang, B., Wang, W., Wiget, S., Petruska, A.J., Chen, X., Hu, C., Hong, A., Folio, D., Ferreira, A., Pane, S., *et al.* (2016). Catalytic Locomotion of Core-Shell Nanowire Motors. *ACS Nano* *10*, 9983-9991.

Lindken, R., Rossi, M., Große, S., and Westerweel, J. (2009). Micro-Particle Image Velocimetry (μ PIV): Recent developments, applications, and guidelines. *Lab Chip* *9*, 2551-2567.

Singh, D.P., Uspal, W.E., Popescu, M.N., Wilson, L.G., and Fischer, P. (2018). Photogravitactic Microswimmers. *Adv. Funct. Mater.* *28*, 1706660.